Am J Physiol Lung Cell Mol Physiol 304: L43–L55, 2013.
First published October 19, 2012; doi:10.1152/ajplung.00093.2012.

A mutation in the β-subunit of ENaC identified in a patient with cystic fibrosis-like symptoms has a gain-of-function effect

Robert Rauh,[1] Daniel Soell,[1] Silke Haerteis,[1] Alexei Diakov,[1] Viatcheslav Nesterov,[1] Bettina Krueger,[1] Heinrich Sticht,[2] and Christoph Korbmacher[1]

[1]*Institut für Zelluläre und Molekulare Physiologie, Friedrich-Alexander-Universität (FAU) Erlangen-Nürnberg, Erlangen, Germany and* [2]*Abteilung für Bioinformatik, Institut für Biochemie, Friedrich-Alexander-Universität (FAU) Erlangen-Nürnberg, Erlangen, Germany*

Submitted 7 March 2012; accepted in final form 17 October 2012

Rauh R, Soell D, Haerteis S, Diakov A, Nesterov V, Krueger B, Sticht H, Korbmacher C. A mutation in the β-subunit of ENaC identified in a patient with cystic fibrosis-like symptoms has a gain-of-function effect. *Am J Physiol Lung Cell Mol Physiol* 304: L43–L55, 2013. First published October 19, 2012; doi:10.1152/ajplung.00093.2012.—In some patients with atypical cystic fibrosis (CF), only one allele of the CF transmembrane conductance regulator (CFTR) gene is affected. Mutations of the epithelial sodium channel (ENaC) may contribute to the pathophysiology of the disease in these patients. To functionally characterize a mutation in the β-subunit of ENaC (βV348M) recently identified in a patient with severe CF-like symptoms (Mutesa et al. 2009), we expressed wild-type (wt) αβγENaC or mutant αβV348MγENaC in *Xenopus laevis* oocytes. The βV348M mutation stimulated amiloride-sensitive whole-cell current (ΔI_{ami}) by ~40% but had no effect on surface expression or single-channel conductance of ENaC. Instead the mutation increased channel open probability (P_o). Proteolytic activation of mutant ENaC by chymotrypsin was reduced compared with that of wt ENaC (~3.0-fold vs. ~4.2-fold), which is consistent with the increased baseline P_o of mutant ENaC. Similarly, the ENaC activator S3969 stimulated mutant ENaC currents to a lesser degree (by ~2.6-fold) than wt ENaC currents (by ~3.5-fold). The gain-of-function effect of the βV348M mutation was confirmed by whole-cell current measurements in HEK293 cells transiently transfected with wt or mutant ENaC. Computational channel modeling in combination with functional expression of different βV348 mutants in oocytes suggests that the βV348M mutation increases channel P_o by destabilizing the closed channel state. Our findings indicate that the gain-of-function effect of the βV348M mutation may contribute to CF pathophysiology by inappropriately increasing sodium and fluid absorption in the respiratory tract.

gain-of-function mutation; *Xenopus laevis* oocyte expression system; electrophysiology; computational channel modeling; sodium transport in cystic fibrosis; epithelial sodium channel

CYSTIC FIBROSIS (CF) is a common autosomal recessive hereditary disease that is usually caused by mutations in the CF transmembrane conductance regulator (CFTR) gene (46). The CFTR gene encodes a Cl^- channel, which is found in the apical membrane of a wide range of epithelial cells (50). Defective CFTR results in reduced apical Cl^- conductance, a typical hallmark of CF epithelia. Patients with CF present with diverse symptoms, e.g., chronic sinopulmonary disease, exocrine pancreatic insufficiency, failure to thrive, or congenital bilateral absence of the vas deferens (13). The large heterogeneity of symptoms and a poor genotype/phenotype correlation suggest that modifier genes exist (12). The genes encoding the β- and γ-subunits of the epithelial sodium channel (ENaC) have been reported to be potential modifier genes in CF (53). Moreover, in some patients with a milder CF phenotype (so-called atypical CF), no CFTR mutations could be identified or only one allele was affected (1, 51). Interestingly, the identified mutations of ENaC include gain-of-function as well as loss-of-function mutations (1, 24, 44, 51), which makes it challenging to develop a concept of how ENaC function may modify CF.

ENaC is the rate-limiting step for sodium absorption in a variety of sodium-absorbing epithelia, e.g., in the lung, distal nephron, distal colon, and sweat and salivary ducts (18, 19, 29). It is a member of the ENaC/degenerin family of non-voltage-gated ion channels. In epithelial tissues, the channel is composed of three homologous subunits (α, β, γ). Each subunit has cytosolic NH_2 and COOH termini and two transmembrane domains that are connected by a large extracellular loop (29). The published crystal structure of the related acid-sensing ion channel (ASIC1) (26, 55) and recent atomic force microscopy data (54) suggest that ENaC is a heterotrimer. In respiratory epithelia, a fine balance between Na^+ absorption via ENaC and Cl^- secretion via CFTR is thought to be necessary to maintain an appropriate airway surface liquid (ASL) volume, which is important for pulmonary mucus clearance (3, 16). In classical CF with defective CFTR, the failure to secrete Cl^- is probably the main cause for ASL volume depletion, which reduces mucociliary clearance and favors bacterial infections. In addition, enhanced sodium absorption may contribute to ASL volume depletion and may aggravate CF symptoms. Indeed, higher ENaC activity has recently been demonstrated in freshly isolated murine alveolar epithelial cells when CFTR expression was reduced or totally absent (35). Importantly, transgenic mice overexpressing β-ENaC in the airways develop a CF-like pulmonary phenotype (37). This demonstrates that, at least in mice, enhanced Na^+ absorption in respiratory epithelia is sufficient to cause CF-like disease. Similarly, knockout of Nedd4–2, a negative regulator of ENaC expression at the plasma membrane, also causes CF-like pulmonary symptoms in mice (2, 30). Preventive amiloride therapy reduces morbidity and mortality in β-ENaC-overexpressing (59) and Nedd4–2 knockout (30) mice. These findings support the hypothesis that ENaC gain-of-function mutations may contribute to CF pathophysiology. Recent studies of a porcine model showed that excised and cultured $CFTR^{-/-}$ and $CFTR^{\Delta F508/\Delta F508}$ airway epithelia did not hyperabsorb Na^+ (9). Moreover, it has been reported that, in differentiated primary cultures of human CF and non-CF respiratory epithelia, the Na^+ channel inhibitor amiloride produced similar reductions in transepithelial conductance and Na^+ absorption, indicating that Na^+ conductance in CF epithelia did not exceed that in non-CF epithelia (25). Thus at present it remains a matter of debate

Address for reprint requests and other correspondence: R. Rauh, Institut für Zelluläre und Molekulare Physiologie, Waldstr. 6, D-91054 Erlangen, Germany (e-mail: robert.rauh@fau.de).

whether enhanced ENaC function contributes to the pathophysiology of CF. It is conceivable that ENaC hyperactivity may play a role in only a subset of patients with CF.

Recently, a mutation in the β-subunit (βV348M) of ENaC has been identified in a patient with severe CF-like symptoms (recurrent respiratory infections, lung colonization by *Pseudomonas aeruginosa*, gastrointestinal symptoms, failure to thrive, diabetes mellitus, and protein energy malnutrition) (39). Moreover, the βV348 residue has been reported to be critical for the stimulatory effect of the novel ENaC activator S3969 (36). These findings suggest that this residue is functionally important and that the identified mutation is likely to alter channel properties. The aim of the present study was to investigate the effects of the βV348M mutation on ENaC function.

MATERIALS AND METHODS

Chemicals and solutions. Unless stated otherwise, chemicals were from Sigma (Taufkirchen, Germany). 2-(trimethylammonium)ethyl methanethiosulphonate bromide (MTSET) was obtained from Toronto Research Chemicals (Toronto, Ontario, Canada); collagenase type II (CLS II), fetal bovine serum, sodium pyruvate and nonessential amino acids were from Biochrom (Berlin, Germany); and Modified Eagle's Medium was from PAA Laboratories (Cölbe, Germany). S3969 (36) was synthesized as described previously (24). The solutions used were: OR2 for isolation of oocytes (in mM: 82.5 NaCl, 2 KCl, 1 $MgCl_2$, 5 HEPES, pH 7.4 with NaOH), a low-Na^+-containing solution for oocyte incubation (in mM: 87 NMDG-Cl, 9 NaCl, 2 KCl, 1.8 $CaCl_2$, 1 $MgCl_2$, 5 HEPES, 100 U/ml penicillin, 100 μg/ml streptomycin, pH 7.4 with Tris), and ND96 as the bath solution for two-electrode voltage-clamp experiments (in mM: 96 NaCl, 2 KCl, 1.8 $CaCl_2$, 1 $MgCl_2$, 5 HEPES, pH 7.4 with Tris). Solutions used for outside-out patch-clamp procedures were: pipette solution (in mM: 90 K-gluconate, 5 NaCl, 2 Mg-ATP, 2 EGTA, 10 HEPES, pH 7.28 with Tris), low-sodium NMDG-Cl bath solution (in mM: 95 NMDG-Cl, 1 NaCl, 4 KCl, 1 $MgCl_2$, 1 $CaCl_2$, 10 HEPES, pH 7.4 with Tris), and high-sodium bath solution (in mM: 95 NaCl, 4 KCl, 1 $MgCl_2$, 1 $CaCl_2$, 10 HEPES, pH 7.4 with Tris). Solutions used for whole-cell voltage clamp on HEK293 cells were: pipette solution [in mM: 130 CsCl, 2 Mg-ATP, 10 HEPES, 5 EGTA-Na (tetrasodium salt), 2 $MgCl_2$, pH 7.2 with Tris], and bath solution (in mM: 160 NaCl, 1 $CaCl_2$, 2 $MgCl_2$, 10 HEPES, pH 7.4 with Tris).

Plasmids. Full-length cDNAs for all human ENaC subunits were cloned in pcDNA3.1 as previously described (1). Linearized plasmids were used as templates for cRNA synthesis using T7 RNA polymerases (mMessage mMachine; Ambion, Austin, TX). To minimize the risk of expression artifacts that may arise from differences in cRNA quality, cRNAs for wild-type (wt) and mutant ENaC were synthesized in parallel, and the experiments were performed using at least two different batches of cRNA. Point mutations were generated by site-directed mutagenesis (QuikChange Site-Directed Mutagenesis Kit; Stratagene, Amsterdam, Netherlands) and confirmed by sequence analysis.

Isolation of oocytes and injection of cRNA. Oocytes were obtained from adult female *Xenopus laevis* in accordance with German legislation, with approval by the animal welfare officer for the University of Erlangen-Nuremberg, and under the governance of the state veterinary health inspectorate. Animals were anesthetized in 0.2% MS222 (ethyl 3-aminobenzoate methanesulfonate salt). Ovarian lobes were obtained by partial ovariectomy, and oocytes were isolated by enzymatic digestion at 19°C for 3–4 h with 600–700 U/ml collagenase type II dissolved in OR2 solution. Isolated oocytes were stored in ND96 supplemented with 100 U/ml penicillin and 100 μg/ml streptomycin to prevent bacterial overgrowth until injection. Defolliculated stage V-VI oocytes were injected (Nanoject II automatic injector; Drummond, Broomall, PA) with 0.5 ng cRNA per subunit of ENaC. The cRNAs were dissolved in RNase-free water, and the total volume injected was 46 nl. To prevent excessive sodium loading of ENaC-expressing oocytes, the injected oocytes were stored until use in a low-Na^+-containing solution (supplemented with 100 U/ml penicillin and 100 μg/ml streptomycin) at 19°C as previously described (21, 24, 44).

HEK293 cell culture and transfection. HEK293 cells were cultured in Modified Eagle's Medium supplemented with 10% fetal bovine serum, 1 mM sodium pyruvate, 1% nonessential amino acids, 100 U/ml penicillin, and 100 μg/ml streptomycin. Cells were transfected with plasmids coding for α-, γ- and β- or βV348M-ENaC 1 day after seeding at a level of ~60% confluence using X-treme Gene HP DNA transfection reagent (Roche Diagnostics, Mannheim, Germany) according to the manufacturer's protocol. The transfection reagent was used in a ratio 1:4. pEGFP-C1 (Invitrogen, Darmstadt, Germany) was cotransfected to identify positively transfected cells in the patch-clamp experiments using fluorescence microscopy. After transfection, medium was supplemented with amiloride (10 μM) to avoid excessive sodium loading of the cells.

Two-electrode voltage clamp. Oocytes were routinely studied 1–2 days after injection using the two-electrode voltage-clamp technique as described previously (45, 58). The oocytes were placed in a small experimental chamber and constantly superfused (2–3 ml/min) at room temperature with ND96 supplemented with amiloride (2 μM). Bath solution exchanges were controlled by an ALA BPS-8 magnetic valve system in combination with a TIB14 interface (both HEKA, Lambrecht, Germany). Voltage-clamp experiments were performed using an OC-725C amplifier (Warner Instruments, Hamden, CT) interfaced via a LIH-1600 (HEKA) to a PC running PULSE 8.67 software (HEKA) for data acquisition and analysis. For continuous whole-cell current recordings, oocytes were routinely clamped at a holding potential of −60 mV. Amiloride-sensitive whole-cell currents (ΔI_{ami}) were determined by washing out amiloride with amiloride-free ND96 and by subtracting the whole-cell current measured in the absence of amiloride from that measured in the presence. Downward current deflections in current traces correspond to inward currents, i.e., movement of positive charge into the cell.

Patch-clamp experiments on oocytes. Single-channel recordings in conventional outside-out patches were essentially performed as described previously (15, 44). Oocytes were routinely studied 2–3 days after injection. Patch pipettes were pulled from borosilicate glass capillaries and had a tip diameter of ~1–1.5 μm after fire polishing. Pipettes were filled with potassium gluconate pipette solution. Seals were routinely formed in a low-Na^+ NMDG-Cl bath solution. In this bath solution, the pipette resistance averaged ~7 MΩ. After seal formation, the bath solution was changed to a high-Na^+ solution. Outside-out patches were routinely voltage clamped at −70 mV, which is close to the calculated reversal potential of Cl^- (E_{Cl} = −77.2 mV) and K^+ (E_K = −79.4 mV) under our experimental conditions. Experiments were performed at room temperature (~23°C). The current level at which all channels are closed was determined in the presence of amiloride (2 μM). Downward current deflections correspond to cell membrane inward currents, i.e., movement of positive charge from the extracellular side to the cytoplasmic side. Single-channel current data were filtered at 1 kHz and digitized at 3 kHz before refiltering at 50 Hz to calculate single-channel current amplitude and channel activity. The current level at which all channels are closed (closed level) was determined in the presence of amiloride (2 μM). Binned amplitude histograms were used to determine the single-channel current amplitude (i) and to estimate channel activity as the product NP_o, where N is the number of channels and P_o is the single-channel open probability (14, 15, 33, 34). To analyze channel gating, we calculated the number of channel transitions per second per apparent number of channels (Transitions × s^{-1} × N_{app}^{-1}) (34). Data analysis was performed using the program Patch for Windows written by Dr. Bernd Letz (HEKA Elektronik, Lambrecht/Pfalz, Germany).

Whole-cell patch-clamp experiments in HEK293 cells. Conventional whole-cell patch-clamp recordings from cultured HEK293 cells were performed at 37°C using an experimental protocol and setup essentially as described previously (41, 42). Green fluorescent protein fluorescence was used to facilitate selection of successfully transfected cells. Only recordings with a clear amiloride response were included in the data analysis (~20% of selected cells did not respond to amiloride). Pipettes were made from borosilicate glass and had a resistance of 3–4 MΩ. Seal resistance was 4–10 GΩ, and series resistance (R_s) was 5–8 MΩ. Membrane capacitance (C_m) and R_s were estimated using the automated capacitance compensation procedure of the EPC-9 amplifier. R_s was compensated by 70%; C_m ranged from 7 to 15 pF. Cells were voltage clamped at a holding potential of −60 mV. Current signals were filtered at 250 Hz and sampled at a rate of 1 kHz. For further analysis and presentation, they were routinely refiltered at 100 Hz. The amiloride-sensitive current (ΔI_{ami}) was determined by subtracting the whole-cell current measured in the presence of amiloride from that measured in the absence of amiloride (2 μM). Current density was calculated as the ratio of ΔI_{ami} to cell membrane capacitance.

Detection of βENaC at the cell surface. Biotinylation experiments were performed essentially as described (14, 22, 23) using 30 oocytes per group. All biotinylation steps were performed on ice. Oocytes were incubated in biotinylation buffer [in mM: 10 triethanolamine, 150 NaCl, 2 $CaCl_2$, EZ-link sulfo-NHS-SSBiotin (1 mg/ml, pH 9.5; Pierce, Rockford, IL)] for 15 min with gentle agitation. The biotinylation reaction was stopped by washing the oocytes twice for 5 min with a quenching buffer (in mM: 192 glycine, 25 Tris, pH 7.5). Oocytes were lysed by passing them five times through a 27-gauge needle in lysis buffer (in mM: 500 NaCl, 5 EDTA, 50 Tris, pH 7.4) supplemented with a protease inhibitor cocktail (Complete Mini EDTA-free protease inhibitor cocktail tablets; Roche Diagnostics) according to manufacturer's instructions. The lysates were centrifuged for 10 min at 1,500 *g*. After addition of 0.5% Triton X-100 and 0.5% Igepal CA-630, supernatants were incubated for 20 min on ice, and 100 μl of Immunopure immobilized Neutravidin beads (Pierce) were added. After overnight incubation at 4°C with overhead rotation, the tubes were centrifuged for 3 min at 1,500 *g*. Supernatants were removed and used for the detection of intracellular βENaC. The remaining beads were washed three times with lysis buffer, and 100 μl of 2× SDS-PAGE sample buffer (Rotiload 1; Roth, Karlsruhe, Germany) were added. Samples were boiled for 5 min at 95°C and centrifuged for 3 min at 20,000 *g* before loading the supernatants on a 10% SDS-PAGE gel. Separated proteins were transferred onto a nitrocellulose membrane by semidry blotting and detected with a primary rabbit anti-human βENaC antibody (1:10,000) (22) and a horseradish peroxidase-labeled secondary goat anti-rabbit antibody (1:50,000; Santa Cruz Biotechnology, Heidelberg, Germany). Absence of intracellular proteins was determined by monitoring the β-actin signal. Densitometric analysis was performed using ImageJ 1.38x (National Institutes of Health, Bethesda, MD).

ENaC modeling. The structural effects of mutating V348 were investigated based on a previous model of ENaC (44) that was generated on the basis of the published crystal structure of ASIC1, which belongs to the ENaC/degenerin gene family (26). According to the conformation of the template, the present model is likely to represent a closed conformation of ENaC. Mutants were generated with the Swiss-PdbViewer (49). Structural analysis and visualization was performed using RasMol (48).

Statistical methods. Data are presented as means ± SE. *N* indicates the number of different batches of oocytes, *n* the number of individual oocytes studied. Statistical significance was assessed using the appropriate version of Student's *t*-test or one-way ANOVA followed by Dunnett's Multiple Comparison test with GraphPad Prism 4.03 for Windows (GraphPad Software, San Diego, CA).

RESULTS

The βV348M mutation stimulates ENaC-mediated whole-cell currents in Xenopus laevis oocytes. To study the effect of the βV348M mutation on ENaC function, we expressed wild-

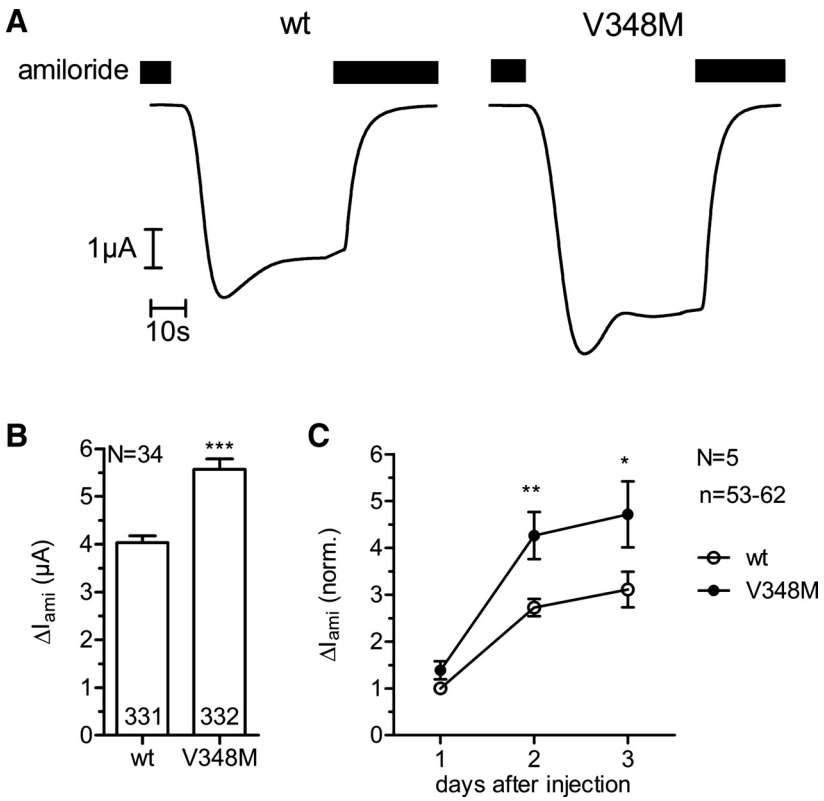

Fig. 1. βV348M mutation stimulates epithelial sodium channel (ENaC). Wild-type αβγENaC (wt) or mutant αβV348MγENaC (V348M) was expressed in *Xenopus laevis* oocytes, and amiloride-sensitive whole-cell currents (ΔI_{ami}) were measured with the two-electrode voltage-clamp technique. *A*: representative whole-cell current traces of a wild-type and a mutant ENaC-expressing oocyte at a holding potential of −60 mV. Amiloride (2 μM) was present in the bath as indicated by the black bars. *B*: summary of similar experiments as shown in *A* performed in wild-type and mutant ENaC-expressing oocytes. *C*: summary of 5 time course measurements of wild-type and mutant ENaC-expressing oocytes. To correct for batch-to-batch variability, current values were normalized to wild-type control on *day 1*. Each data point represents mean ΔI_{ami} measured in 53–62 oocytes. *N* indicates the number of different batches of oocytes; *n* or numbers in columns indicate the number of individual oocytes. $^*P < 0.05$, $^{**}P < 0.01$, $^{***}P < 0.001$, unpaired *t*-test.

type αβγENaC or mutant αβV348Mγ ENaC in *Xenopus laevis* oocytes and determined amiloride-sensitive whole-cell currents (ΔI_{ami}) with two-electrode voltage clamp. Figure 1*A* shows typical whole-cell current traces recorded from a wild-type and a mutant ENaC-expressing oocyte. In 34 different batches of oocytes, ΔI_{ami} averaged 4.0 ± 0.14 μA in αβγENaC-expressing control oocytes (n = 331) and 5.6 ± 0.22 μA in αβV348Mγ ENaC-expressing oocytes (n = 332, $P < 0.001$) (Fig. 1*B*). Thus on average the βV348M mutation stimulated the ENaC-mediated whole-cell Na^+ current by ~38%. In five batches of oocytes, we measured ΔI_{ami} on three consecutive days following cRNA injection (Fig. 1*C*). In wild-type and mutant ENaC-expressing oocytes, ΔI_{ami} increased from *day 1* to *day 3*, which demonstrates that with longer incubation periods more ENaC protein is synthesized and delivered to the plasma membrane (27). Importantly, on *days 2* and *3*, ΔI_{ami} was significantly higher in mutant than in wild-type ENaC-expressing oocytes, confirming that the stimulatory effect of the βV348M mutation on ENaC function is a robust phenomenon. In conclusion, our results demonstrate that the βV348M mutation causes an increase in ENaC function.

βV348M increases channel open probability. The stimulatory effect of the βV348M mutation can result from an increased density of channels expressed at the plasma membrane, a higher channel open probability (P_o), or a higher single-channel conductance. To test whether the βV348M mutation increases the average channel P_o, we introduced a βS520C point mutation into the wild-type and mutant β-subunit (14, 22, 24, 36). Binding of the sulfhydryl reagent MTSET to this cysteine stabilizes the open state of the channel, thereby shifting channel P_o close to 1 (28, 52). Therefore, the ratio of baseline ΔI_{ami} to ΔI_{ami} after activation with MTSET provides an estimate of the average channel P_o before the application of MTSET. Application of MTSET (1 mM) on αβS520Cγ ENaC-expressing oocytes stimulated ΔI_{ami} ~4.2-fold (Fig. 2), which indicates a P_o of ~0.24 before the application of MTSET. ΔI_{ami} of αβV348M-S520Cγ ENaC-expressing oocytes was on average ~43% higher than that of αβS520Cγ ENaC-expressing control oocytes, confirming a stimulatory effect of the βV348M mutation in this set of experiments. Application of MTSET to αβV348M-S520Cγ ENaC-expressing oocytes stimulated ΔI_{ami} ~3.0-fold, which indicates an average P_o of ~0.33 before the application of MTSET. These findings support the concept that a higher P_o of mutant ENaC contributes to the gain-of-function effect of the mutation. Interestingly, ΔI_{ami} levels of αβS520Cγ ENaC- and αβV348M-S520Cγ ENaC-expressing oocytes after MTSET stimulation were comparable. Under the assumption that the single-channel conductance is not affected by the V348M mutation (see below), these findings indicate that an increase in channel surface expression does not contribute to the gain-of-function effect of the βV348M mutation.

To investigate whether the βV348M mutation alters the single-channel conductance of ENaC and to confirm that it increases P_o, we performed single-channel recordings using outside-out patches obtained from oocytes expressing wild-type αβγENaC or mutant αβV348Mγ ENaC. Figure 3*A* shows typical single-channel current traces recorded at different holding potentials. The corresponding *I*/*V* plots are shown in Fig. 3*B*. The Goldman-Hodgkin-Katz fits of the data suggest that the wild-type and the mutant channel are sodium selective. In similar experiments, as shown in Fig. 3, the single-channel

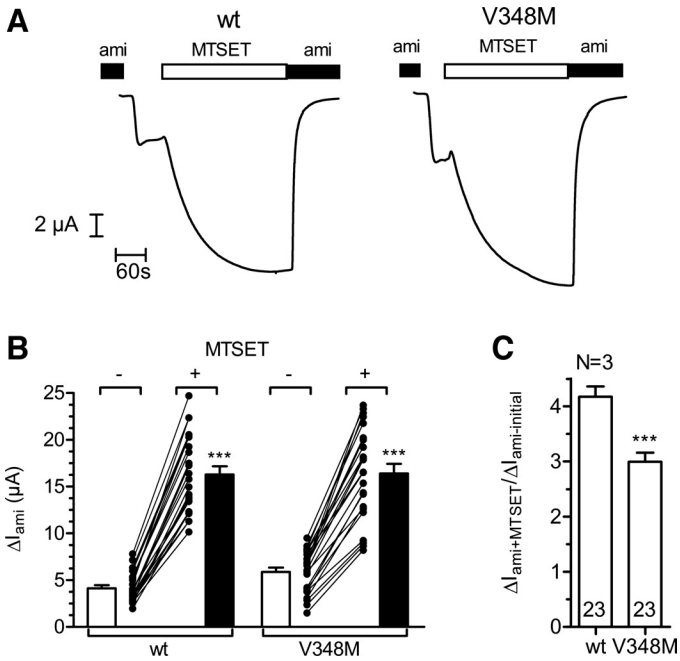

Fig. 2. βV348M mutation increases average open probability (P_o). *A*: representative whole-cell current traces of an αβS520Cγ-ENaC (wt)- and an αβV348M-S520Cγ-ENaC (V348M)-expressing oocyte at a holding potential of −60 mV. Amiloride (2 μM) and 2-(trimethylammonium)ethyl methanethiosulphonate bromide (MTSET) (1 mM) were present in the bath as indicated by the black and white bars, respectively. MTSET can increase P_o of channels containing the βS520C-mutation to nearly 1. *B*: summary of similar experiments as shown in *A* performed in oocytes from 3 different batches. *C*: same data as shown in *B* but normalized to the corresponding control value before MTSET application to demonstrate the relative stimulatory effect of MTSET on ΔI_{ami}. *N* indicates the number of different batches of oocytes; numbers in columns indicate the number of individual oocytes. ***$P < 0.001$, paired (*B*) or unpaired (*C*) *t*-test.

conductance of the mutant ENaC averaged 5.20 ± 0.04 pS (n = 7), which is only marginally lower than that of wild-type ENaC averaging 5.4 ± 0.05 pS (n = 6, $P < 0.01$). These single-channel conductance values are in good agreement with those previously reported for human ENaC (24, 44, 54). Thus we have no evidence that an increased single-channel conductance or an altered ion selectivity contribute to the gain-of-function effect of the βV348M mutation.

Importantly, our single-channel current recordings demonstrate that the βV348M mutation alters the gating kinetics of ENaC. The representative current traces shown in Fig. 3*A* suggest that the gating kinetics of mutant ENaC are slower than those of wild-type ENaC. To further analyze a possible effect of the mutation on channel gating, we performed additional continuous single-channel recordings at a holding potential of −70 mV as illustrated in Fig. 4. At the beginning of these recordings, amiloride was present in the bath solution to determine the current level at which all channels are closed. Washout of amiloride resulted in the appearance of single-channel current activity. In the absence of amiloride, the average NP_o of the mutant ENaC showed a nonsignificant trend to be higher than the average NP_o of wild-type ENaC (Fig. 4*C*). The maximal number of apparent channel levels (N_{app}) observed in outside-out patches with mutant ENaC was similar to that observed in outside-out patches with wild-type ENaC (Fig. 4*D*). By calculating the ratio of NP_o to N_{app}, we

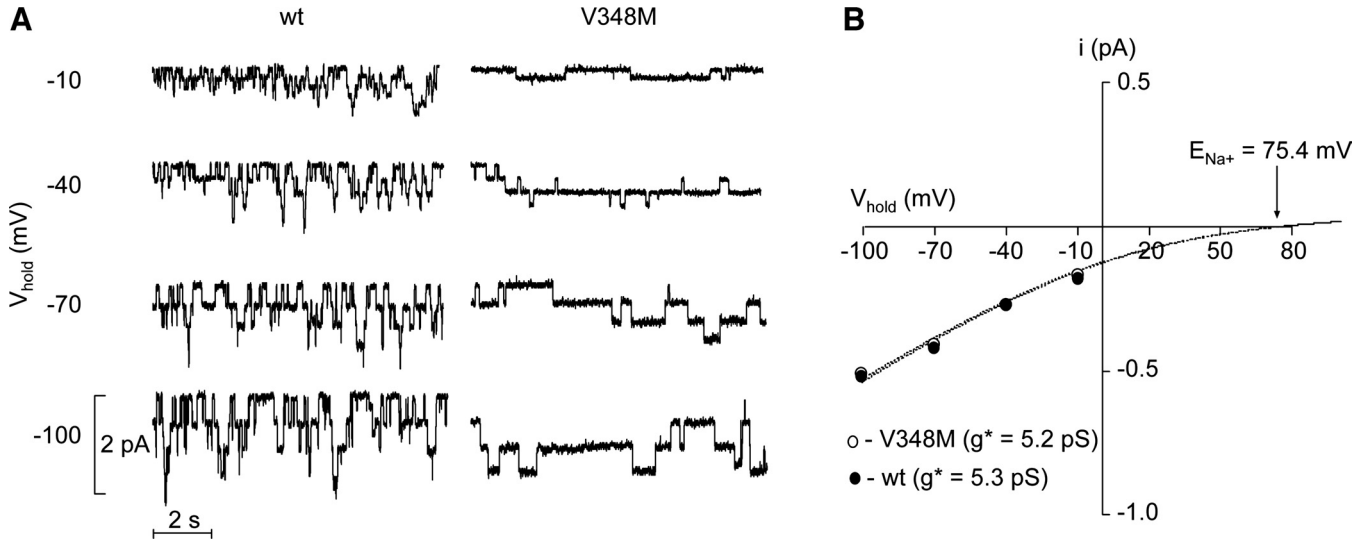

Fig. 3. Effect of the V348M mutation on the single-channel conductance of ENaC. *A*: representative single-channel current traces recorded at different holding potentials (V_{hold}) using outside-out patches from an αβγENaC (wt)- and an αβV348MγENaC (V348M)-expressing oocyte. *B*: single-channel *I/V* relations obtained from the recordings shown in *A*. *I/V* data were fitted using the Goldman-Hodgkin-Katz (GHK) equation (dashed lines). E_{Na+} represents the calculated equilibrium potential under our experimental conditions. *g** represents the single-channel conductance obtained from the GHK fits.

estimated the single-channel P_o in several recordings similar to those shown in Fig. 4, *A* and *B*. On average the P_o of mutant ENaC ($n = 11$) was ~61% higher than that of wild-type ENaC ($n = 11$; $P < 0.05$; Fig. 4*E*). To further quantify the effect of the βV348M on channel gating, we counted the overall number of channel transitions per time as previously described (34). The average number of channel transitions per second and per N_{app} was largely reduced in outside-out patches with mutant ENaC compared with outside-out patches with wild-type ENaC (Fig. 4*F*). Thus, the V348M mutation reduces the frequency of gating events, which is likely to contribute to the observed increase in P_o. In summary, our single-channel data confirm that the βV348M mutation causes a gain-of-function effect by increasing channel P_o.

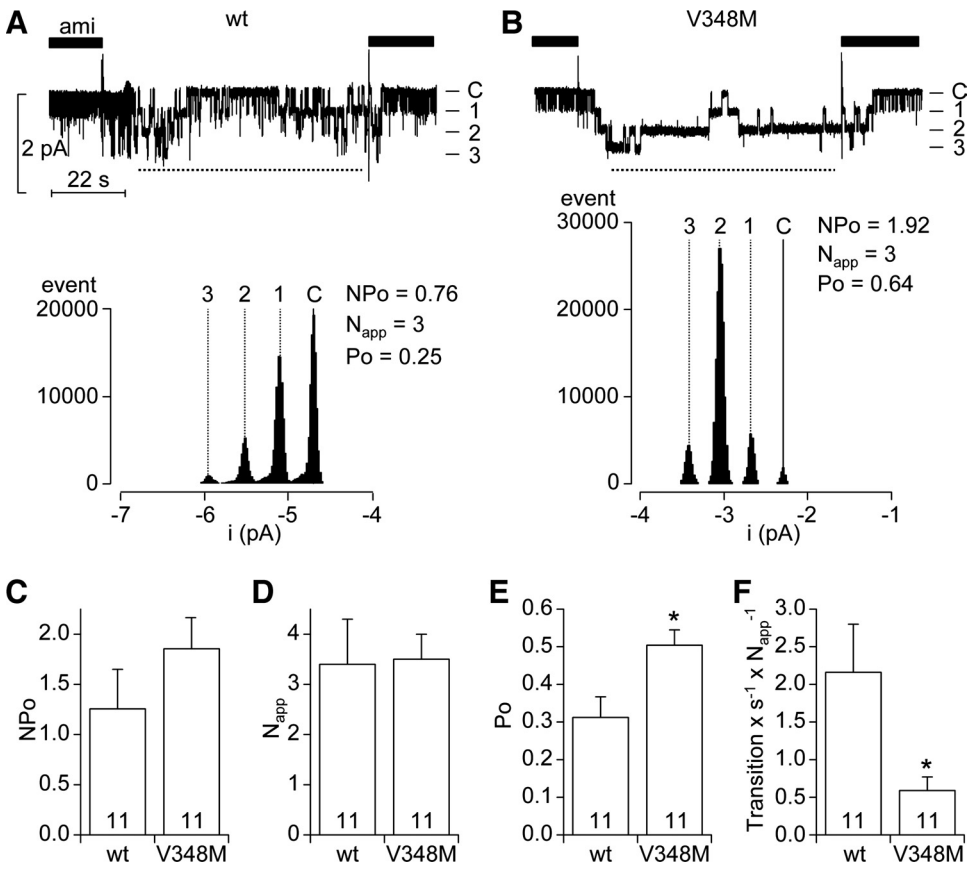

Fig. 4. The V348M mutation increases single-channel P_o. *A* and *B*: representative single-channel current traces from outside-out patches containing αβγENaC (wt, *A*) or αβV348MγENaC (V348M, *B*) recorded at a holding potential of −70 mV. The current level at which all channels are closed (*C*) was determined in the presence of amiloride (ami, 2 μM, black bars above traces). Channel open levels, NP_o, and the maximal number of apparent channel levels (N_{app}) were determined using binned current amplitude histograms (shown below each trace) derived from the time periods indicated by broken lines. *C* and *D*: summary of NP_o (*C*) and N_{app} (*D*) values obtained from similar experiments as shown in *A* and *B*. *E*: from the data shown in *C* and *D*, an apparent P_o was calculated for each recording as the ratio of NP_o to N_{app}. *F*: number of channel transitions per second and per N_{app} (Transition × $s^{-1} \times N_{app}^{-1}$). Numbers in columns indicate the number of individual outside-out patches. *$P < 0.05$, unpaired *t*-test.

Relative activation of ΔI_{ami} by chymotrypsin is reduced in mutant ENaC. ENaC can be activated by serine proteases, e.g., chymotrypsin (7, 8, 10, 14, 21, 31, 43, 44, 47). To test whether the βV348M mutation alters the responsiveness of the channel to proteases, we measured the effect of chymotrypsin on ΔI_{ami} in wild-type αβγENaC- and in mutant αβV348Mγ ENaC-expressing oocytes. Baseline ΔI_{ami} of mutant ENaC-expressing oocytes was on average ~36% larger than that of wild-type ENaC-expressing control oocytes, consistent with the results reported above. Application of chymotrypsin (2 μg/ml) on wild-type ENaC-expressing oocytes stimulated ΔI_{ami} ~4.2-fold (Fig. 5), which is similar to the stimulatory effect observed with MTSET in oocytes expressing αβS520Cγ ENaC without the βV348M mutation. In contrast, application of chymotrypsin on mutant ENaC-expressing oocytes stimulated ΔI_{ami} by only ~3.0-fold. This is consistent with the reduced stimulatory effect of MTSET on oocytes expressing αβV348M-S520Cγ ENaC. The finding that the relative activation of mutant ENaC by chymotrypsin is lower than that of wild-type ENaC indicates that the average channel P_o of the mutant channel is increased. After proteolytic activation, ΔI_{ami} reached a similar level in wild-type and mutant ENaC-expressing oocytes. Collectively, these findings are in good agreement with the findings obtained in the experiments with MTSET and with our single-channel data. They further support the conclusion that the gain-of-function effect of the βV348M mutation is not caused by an increase in channel surface expression but by an increase in average channel P_o.

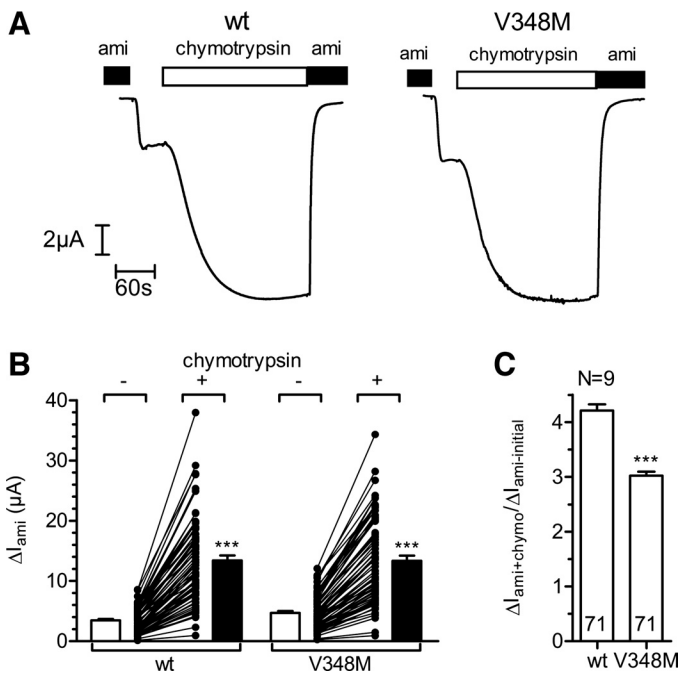

Fig. 5. Relative activation of ΔI_{ami} by chymotrypsin is reduced in mutant ENaC. *A*: representative whole-cell current traces of an αβγ-ENaC (wt)- and an αβV348Mγ-ENaC (V348M)-expressing oocyte at a holding potential of −60 mV. Amiloride (2 μM) and chymotrypsin (2 μg/ml) were present in the bath as indicated by the black and white bars, respectively. *B*: summary of similar experiments as shown in *A* performed in oocytes from 9 different batches. *C*: same data as shown in *B* but normalized to the corresponding control value before chymotrypsin application to demonstrate the relative stimulatory effect of chymotrypsin on ΔI_{ami}. *N* indicates the number of different batches of oocytes; numbers in columns indicate the number of individual oocytes. ***$P < 0.001$, paired (*B*) or unpaired (*C*) *t*-test.

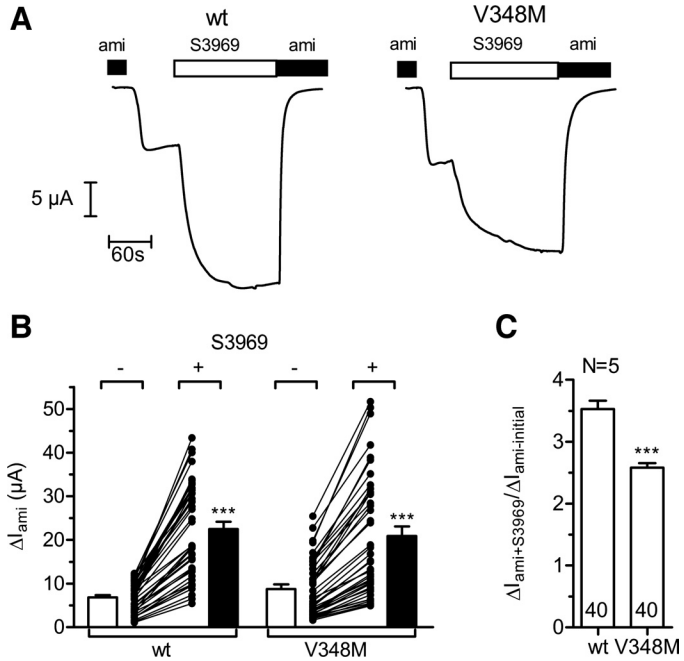

Fig. 6. Stimulatory effect of S3969 on mutant ENaC is reduced. *A*: representative whole-cell current traces of an αβγ-ENaC (wt)- and an αβV348Mγ-ENaC (V348M)-expressing oocyte at a holding potential of −60 mV. Amiloride (2 μM) and S3969 (10 μM) were present in the bath as indicated by the black and white bars, respectively. *B*: summary of similar experiments as shown in *A* performed in oocytes from 5 different batches. *C*: same data as shown in *B* but normalized to the corresponding control value before S3969 application to demonstrate the relative stimulatory effect of S3969 on ΔI_{ami}. *N* indicates the number of different batches of oocytes; numbers in columns indicate the number of individual oocytes. ***$P < 0.001$, paired (*B*) or unpaired (*C*) *t*-test.

The ENaC activator S3969 stimulates mutant ENaC less than wild-type ENaC. Recently, S3969 has been identified as a novel small molecule activator of ENaC (36). At present, the precise mechanism by which S3969 activates ENaC is unknown. However, it has been reported that deletion of V348 in human βENaC abolished the stimulatory effect of the activator. Therefore, we wanted to know whether the βV348M

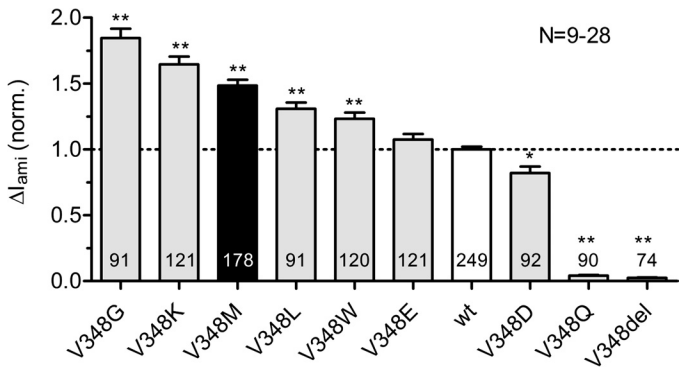

Fig. 7. Amino acid substitutions show diverse effects on ENaC function. ΔI_{ami} was measured in oocytes expressing different mutants as indicated below the columns. To pool data from different batches of oocytes, individual ΔI_{ami} values were normalized to the mean ΔI_{ami} of the corresponding wild-type ENaC (wt)-expressing control oocytes. *N* indicates the number of different batches of oocytes. Numbers in or above columns indicate the total number of oocytes. *$P < 0.05$, **$P < 0.01$, ANOVA followed by Dunnett's multiple-comparison test vs. wild-type control.

mutation reduces the stimulatory effect of S3969. In this set of experiments, ΔI_{ami} of mutant ENaC-expressing oocytes was on average ~29% higher than that of wild-type ENaC-expressing oocytes, consistent with a gain-of-function effect of the βV348M mutation. Application of S3969 (10 μM) on wild-type ENaC-expressing oocytes activated ΔI_{ami} ~3.5-fold (Fig. 6). In contrast, superfusion of mutant ENaC-expressing oocytes with S3969 stimulated ΔI_{ami} ~2.6-fold. Thus the stimulatory effect of S3969 on mutant ENaC is smaller than that on wild-type ENaC. Overall the stimulatory effect of S3969 on both wild-type and mutant ENaC was lower than that of MTSET and chymotrypsin. This indicates that S3969, in contrast to MTSET and chymotrypsin, does not fully activate the channel, which is in agreement with the findings of Lu et al. (36). Nevertheless, our finding that the βV348M mutation significantly reduces the stimulatory effect of S3969 is consistent with the interpretation that the mutation increases average channel P_o.

Different amino acid substitutions at residue β348 show diverse effects on ENaC function. In an additional series of experiments, we investigated whether varying size or charge of residue 348 in βENaC systematically alters ENaC function. We substituted the wild-type valine in position 348 with amino acids of different size or charge and expressed the individual mutants in oocytes. The results summarized in Fig. 7 demonstrate that, in addition to the V348M mutation, four other mutations (V348G, V348K, V348L, V348W) caused a gain-of-function effect with a significantly larger ΔI_{ami} than that for wild-type ENaC. Interestingly, both the small and nonpolar amino acid glycine (V348G) and the large and positively charged lysine (V348K) stimulated ΔI_{ami} more than the nonpolar methionine (V348M) with an intermediate size. The nonpolar leucine (V348L) and the nonpolar tryptophan (V348W) stimulated ENaC less than methionine (V348M). The negatively charged glutamic acid (V348E) had no effect on ENaC function, whereas the negatively charged aspartic acid (V348D) mediated a small but significant inhibitory effect. Interestingly, replacing valine by the polar glutamine (V348Q) or deleting the valine residue (V348del) nearly abolished ENaC function. To test whether these differences result from differences in protein expression, we detected intracellular and biotinylated membrane βENaC levels by Western blot analysis (Fig. 8). Intracellular βENaC protein expression levels

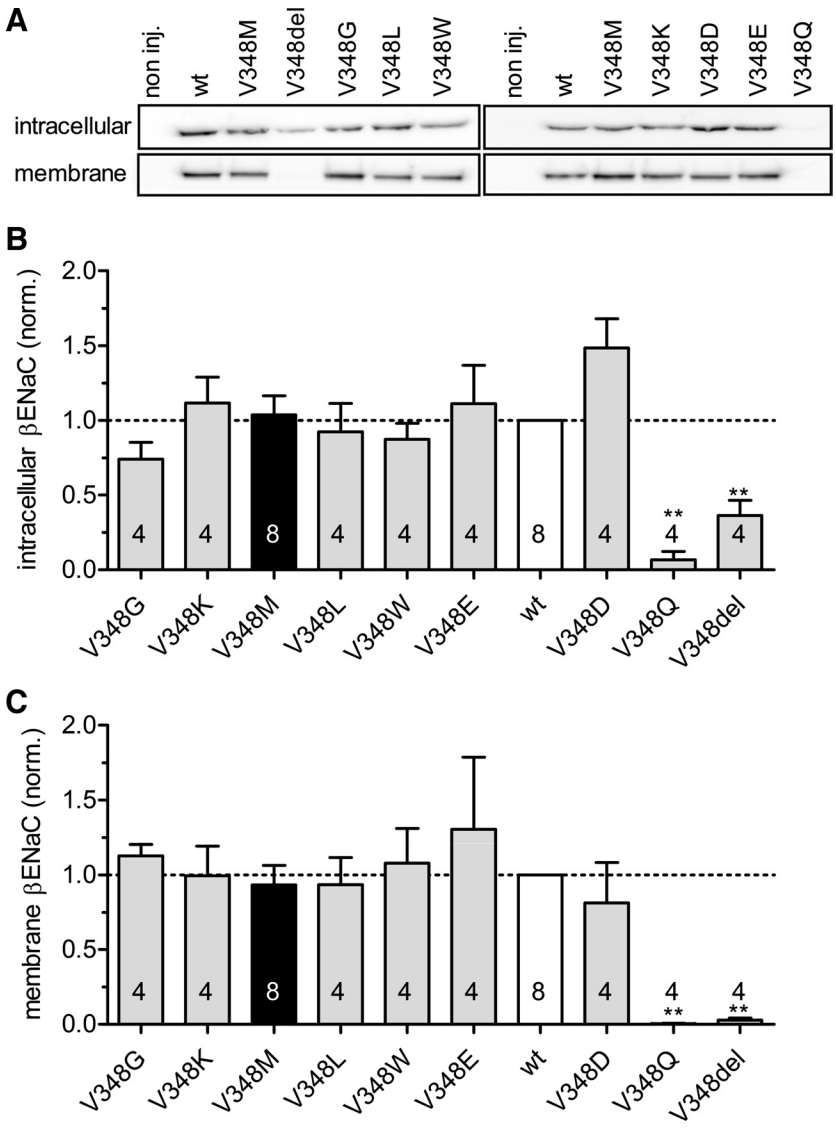

Fig. 8. Effect of different mutations on intracellular and membrane βENaC protein expression. Oocytes were injected with cRNA for wild-type (wt) ENaC or different ENaC mutants as indicated and incubated for 2 days. Intracellular and surface-expressed membrane protein was separated by SDS-PAGE, and βENaC was detected with a specific antibody. *A*: representative Western blots from a batch of oocytes. *B* and *C*: densitometric analysis of 4 similar Western blots as shown in *A*. To correct for batch-to-batch variability, data were normalized to wild-type control. In addition, signals in *B* were normalized to a β-actin loading control. Numbers in or above columns indicate the number of oocyte batches. $^{**}P < 0.01$, ANOVA followed by Dunnett's multiple-comparison test vs. wild-type control.

of the two mutants with the strongest inhibitory effect (V348Q and V348del) were largely reduced (Fig. 8, *A* and *B*), and the corresponding membrane expression signals were hardly distinguishable from background signals (Fig. 8, *A* and *C*). This indicates that a decrease in protein and hence channel surface expression is responsible for the large loss-of-function effect of these two mutations. In contrast, the protein expression level of the other mutants was similar to that of wild-type βENaC both at the plasma membrane and intracellularly. Thus, in these other mutants, the differences in ΔI_{ami} are probably not the result of differences in channel protein expression but are likely to be caused by differences in channel P_o. To test this, we activated all mutants with chymotrypsin, with the exception of the V348Q and V348del mutants, which were not sufficiently expressed to be tested. As shown in Fig. 9*A*, application of chymotrypsin had a large stimulatory effect on ΔI_{ami} in all mutants tested. Under the assumption that chymotrypsin maximally activates ENaC, different average P_o values of the mutant channels should become apparent by differences in the relative activation of ΔI_{ami} by chymotrypsin. Figure 9*B* compares the normalized baseline ΔI_{ami} before chymotrypsin activation with the relative activation of ΔI_{ami} by chymotrypsin.

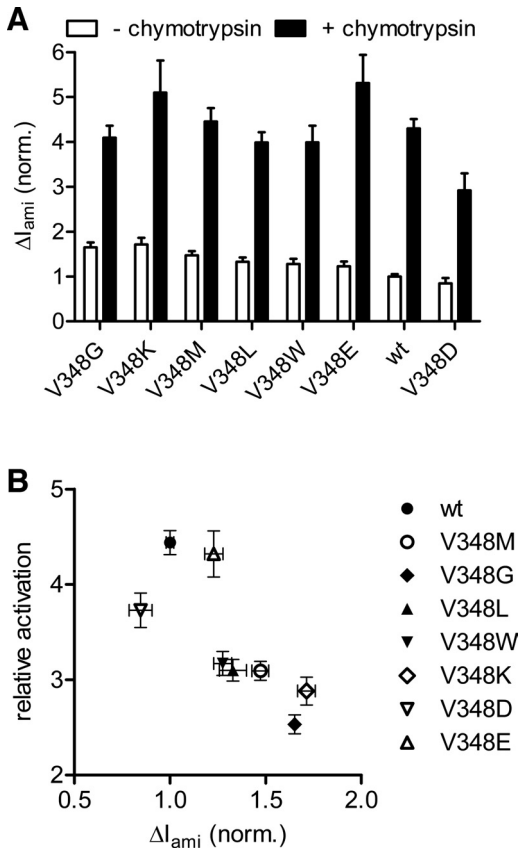

Fig. 9. Effect of chymotrypsin on different mutants. *A*: wild-type (wt) ENaC and different mutants were expressed in oocytes, and ΔI_{ami} was measured with two-electrode voltage-clamp technique. ENaC was activated with chymotrypsin as shown in Fig. 3. Data were pooled from 47 oocytes for wild-type and βV348M-ENaC and from 21–24 oocytes for the remaining mutants. To correct for batch-to-batch variability, data were normalized to mean ΔI_{ami} of wild-type ENaC-expressing oocytes before chymotrypsin activation. *B*: same data as in *A*. The relative chymotrypsin activation was calculated as the ratio of ΔI_{ami} after and before chymotrypsin activation and plotted against basal ΔI_{ami} before chymotrypsin activation.

This figure demonstrates that a higher baseline ΔI_{ami} is related to a lower relative activation by chymotrypsin. This supports the conclusion that the higher baseline currents observed for some of the mutant channels are caused by a higher average P_o before chymotrypsin activation. In summary, our data demonstrate that, in most cases, substitution of the βV348 residue by another amino acid affects channel function by altering average channel P_o. Only in some cases, with largely reduced ENaC currents (V348Q and V348del mutants), the loss-of-function effect was caused by reduced channel surface expression.

To better understand the effects of different amino acid substitutions at βV348, we used computational ENaC modeling according to the crystal structure of ASIC1 (26). Structural analysis of the trimeric ENaC model (Fig. 10*A*) reveals that V348 of the β-subunit is located within a globular domain (termed palm domain) that is located proximal to the membrane (Fig. 10*B*). Interestingly, our model indicates that V348 forms interactions not only within the palm domain but also with the residue M90, which is located in the linker between the palm and the β-ball domain (Figs. 10*B* and 11*A*). Molecular modeling reveals that the majority of the mutations investigated destabilize the structure of the closed ENaC for the following reasons: The lack of the side chain in the V348G mutant results in a loss of the contacts to M90 (Fig. 11B), thereby reducing the stability of the corresponding region. A mutation to lysine (V348K) is unfavorable because of steric clashes with M90 and electrostatic repulsion with K350 (Fig. 11*C*). Clashes of residue 348 with M90 are also observed for V348M (Fig. 11*D*), as well as V348L and V348W (data not shown). In summary, all mutants described above are either characterized by a loss of contact with M90 or by steric clashes with M90. Both effects are energetically unfavorable and are expected to destabilize the interaction between the palm and the β-ball domain (Fig. 10*B*). In contrast, a mutation to glutamate or aspartate allows the formation of a novel stabilizing salt-bridge with K350 (Fig. 11*E*). This may explain why mutating valine to glutamate or aspartate in this position has no stimulatory effect on the channel. Interestingly, the same type of interaction is also observed in the crystal structure of the homologous ASIC1 channel (Fig. 11*F*).

The βV348M mutation stimulates ENaC-mediated whole-cell currents in HEK293 cells. To rule out that the gain-of-function effect of the βV348M mutation is limited to the *Xenopus laevis* oocyte expression system, we transiently transfected HEK293 cells with wild-type αβγENaC or mutant αβV348MγENaC and measured amiloride-sensitive whole-cell currents using the patch-clamp technique. Figure 12A shows representative whole-cell current recordings from a cell expressing wild-type ENaC and a cell expressing mutant ENaC. ΔI_{ami} averaged 85 ± 15 pA ($n = 15$) in wild-type ENaC-expressing cells and 157 ± 26 pA ($n = 12$, $P < 0.05$) in mutant ENaC-expressing cells. To correct for differences in cell size, current density was calculated. Current density averaged 8.0 ± 1.3 pA/pF ($n = 15$) in wild-type ENaC-expressing cells and 14.8 ± 2.4 pA/pF ($n = 12$, $P < 0.05$) in mutant ENaC-expressing cells (Fig. 12*B*). These results indicate that the βV348M mutation also causes a gain-of-function effect in mammalian cells.

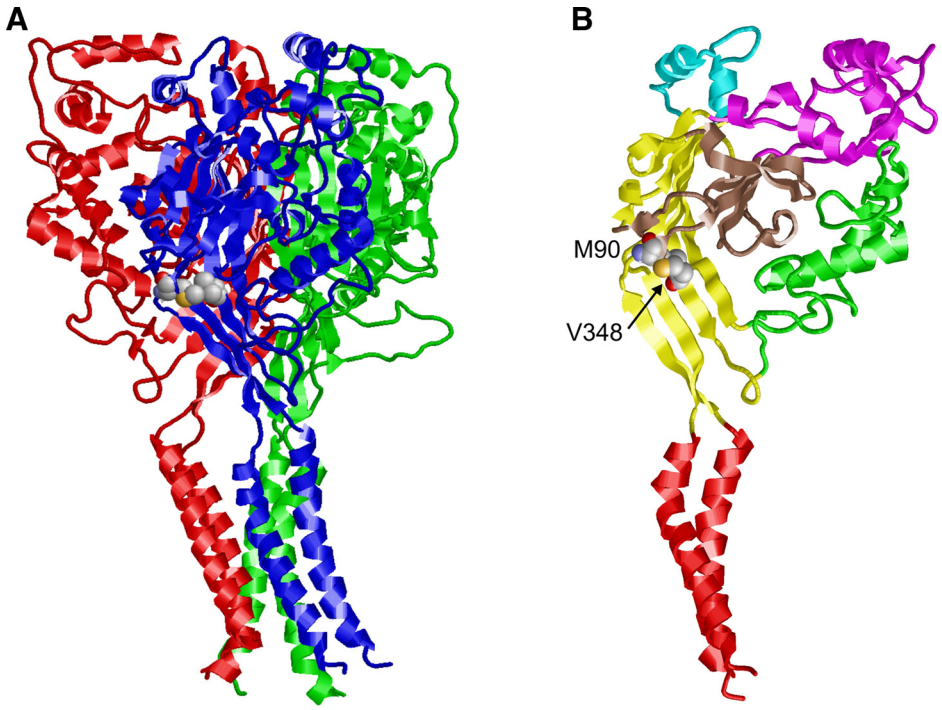

Fig. 10. *A*: model of the trimeric ENaC in the closed conformation. The β-subunit is shown in blue, and residues V348 and M90 are shown in space-filled presentation. *B*: structure of the β-subunit highlighting the domain architecture of ENaC. The domains are defined according to Jasti et al. 2007 and are colored as follows: transmembrane (red), palm (yellow), β-ball (brown), finger (magenta), knuckle (cyan), and thumb (green) domain.

DISCUSSION

In the present study, we investigated the effect of a mutation in βENaC (βV348M) on channel function. To the best of our knowledge, this is the first report on the functional effects of this mutation identified in a patient with severe CF-like symptoms (39). In the *Xenopus laevis* oocyte expression system, we found that the βV348M mutation stimulated ENaC whole-cell currents by ~40%. Using different experimental approaches, including single-channel recordings, we demonstrated that this gain-of-function effect is caused by an increased P_o of the mutant channel. Moreover, we used transiently transfected HEK293 cells to confirm the gain-of-function effect of the βV348M mutation in a mammalian expression system. Our findings suggest that the gain-of-function effect of the βV348M mutation may contribute to CF pathophysiology by inappropriately increasing sodium and fluid absorption in the respiratory tract of affected patients.

Functional testing of the effect of the βV348M-ENaC mutation in the present study was performed in *Xenopus laevis*

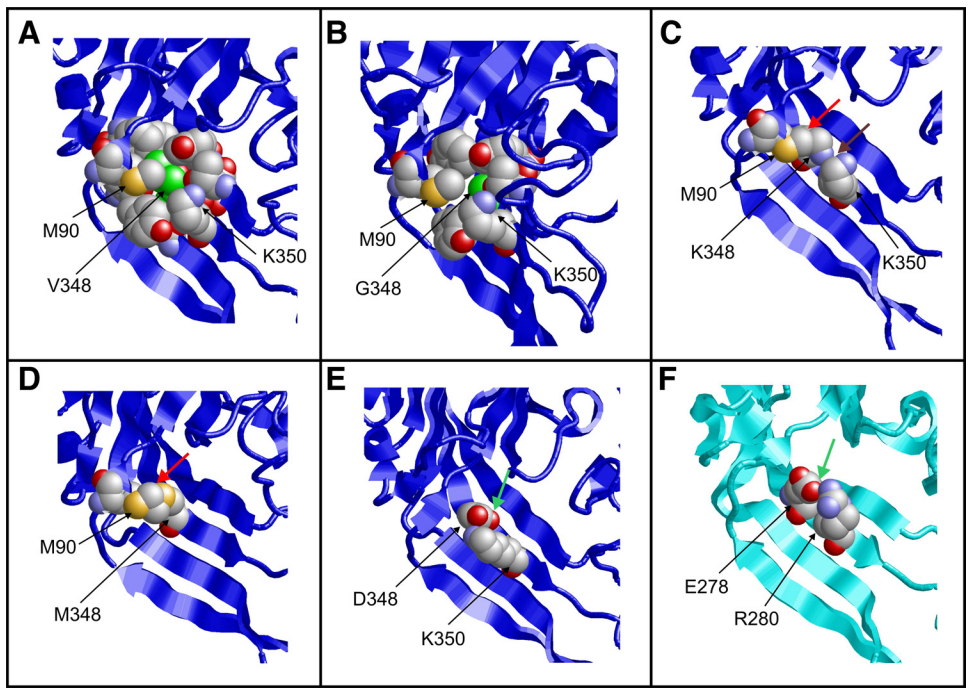

Fig. 11. Detailed view of the V348 mutation site. *A*: site of mutation in the wild-type structure: V348 is shown in green, and the spatially adjacent residues are shown in space-filled presentation. Residues M90 and K350, which are important with respect to the mutants, are labeled. *B*: same view as in *A* for the V348G mutation. Note the loss of packing between G348 (green) and M90. *C*: V348K (K348) results in steric clashes with M90 (red arrow) and electrostatic repulsion with K350 (brown arrow). *D*: V348M (M348) forms clashes with M90 (red arrow). *E*: V348D (D348) forms a novel salt-bridge with K350 (green arrow). *F*: E278-R280 salt-bridge in the crystal structure of the homologous acid-sensing ion channel. The additional residues lining the pocket around residue 348 were omitted in *C*–*F* to enhance the clarity of the presentation.

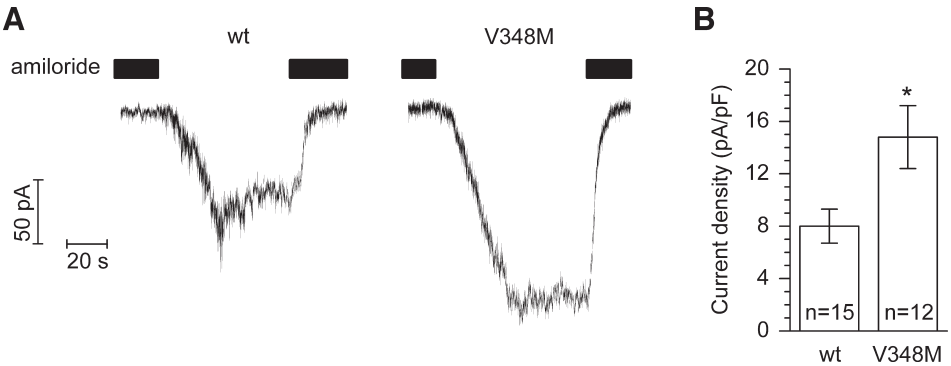

Fig. 12. The βV348M mutation stimulates ENaC in HEK293 cells. HEK293 cells were transiently transfected with wild-type αβγENaC (wt) or mutant αβV348MγENaC (V348M), and amiloride-sensitive whole-cell currents (ΔI_{ami}) were measured using a conventional patch-clamp technique. *A*: representative whole-cell current traces recorded from a wild-type and a mutant ENaC-expressing HEK293 cell at a holding potential of −60 mV. Amiloride (2 μM) was present in the bath as indicated by the black bars. *B*: summary of similar experiments as shown in *A*. To correct for cell size, current density (pA/pF) was calculated. Numbers in columns indicate the number of individual cells. $^*P < 0.05$, unpaired *t*-test.

oocytes, a well-established heterologous expression system for the investigation of ion channels. The use of the oocyte expression system to evaluate the effect of a mutation on channel function requires some precautions to avoid misinterpretation of data. In particular, the batch-to-batch variability of channel expression in oocytes is a well-known phenomenon. To address this, we systematically used matched oocytes from the same batch when comparing the activity of wild-type and mutant channels and repeated the experiments in several batches of oocytes. There is also a batch-to-batch variability in cRNA quality, which may have an impact on protein expression levels and thus whole-cell currents. To minimize the risk of expression artifacts, we synthesized all cRNAs for wild-type and corresponding mutants in parallel, and experiments were repeated with at least two different batches of cRNA. Importantly, we checked protein expression by Western blot analysis and confirmed that the expression levels of wild-type and βV348M-ENaC were similar. The importance of verifying protein expression levels is further illustrated by the finding that the loss-of-function effect of the V348Q and the V348del mutation could be attributed to reduced protein expression of the mutant channels.

We estimated average channel P_o by comparing whole-cell currents after activation of βS520C-ENaC by MTSET to those before activation. With this well-established approach (14, 20, 22, 24, 36), P_o can be estimated under the assumption that all channels are fully activated by MTSET. We previously observed in outside-out patches from oocytes expressing rat αβS518CγENaC (corresponds to human αβS520CγENaC) that MTSET increased the P_o of active channels in the patch close to one and that subsequent application of trypsin was able to activate additional so-called near-silent channels (14). This suggested that activation of near-silent channels requires proteolytic processing of the channel and that MTSET is not able to activate near-silent channels in the same way as trypsin. In contrast, in the present study, MTSET stimulated ENaC to the same extent as chymotrypsin, known to fully activate ENaC, including the recruitment of near-silent channels (44). This indicates that MTSET not only increases the P_o of channels that are already active but can also activate a population of near-silent channels. This different response of human ENaC to MTSET compared with that of rat ENaC (14) may be explained by species-specific differences of ENaC gating (29). MTSET is thought to bind to the channel only when it is in the open conformation (28, 52). Therefore, near-silent channels are unlikely to be activated by MTSET unless they occasionally show spontaneous openings that are long enough for MTSET to act on the channel (14). It is conceivable that near-silent human ENaC opens more frequently and with slightly longer open times than rat ENaC, which may explain its greater responsiveness to MTSET.

In the present study, chymotrypsin activated wild-type and βV348M-ENaC ~4.2-fold and ~3.0-fold, respectively. However, in previous studies on primary human nasal epithelia (17) or human bronchial epithelial cells (4, 11), trypsin failed to activate ENaC, which suggests that in these epithelia ENaC is already fully cleaved and active under resting conditions. In the oocyte expression system, the current levels of wild-type and βV348M-ENaC were similar after full stimulation with chymotrypsin. Thus, in respiratory epithelia with high protease activity and full proteolytic activation of all ENaCs present at the plasma membrane, the βV348M mutation may not result in a gain-of-function phenotype. However, it has been demonstrated that the effect of trypsin on ENaC in cell layers of respiratory epithelia depends on the experimental conditions used (40, 56). Prolonged equilibration periods in the Ussing chamber are thought to wash out endogenous protease inhibitors from the ASL, leading to disinhibition of proteases and hence to proteolytic ENaC activation. In contrast, shortly after changing the epithelial cell layers from the air-liquid interface to the Ussing chambers, trypsin has been shown to have a stimulatory effect on ENaC (5, 40). This latter situation is likely to reflect the situation in vivo at least under certain physiological conditions. Thus the gain-of-function effect of the V348M mutation may well be relevant in native respiratory epithelia.

The presence of V348 in βENaC was reported by Lu et al. (36) to be essential for the stimulatory effect of the novel small molecule ENaC activator S3969. This was concluded from the finding that deletion of βV348 abolished the stimulatory effect of S3969 on ENaC. We were unable to reproduce this finding because of an insufficient expression of the βV348del mutant at the oocyte membrane. We confirmed the stimulatory effect of S3969 on wild-type ENaC described by Lu et al. (36), but

the stimulatory effects of chymotrypsin and MTSET on ENaC were larger than that of S3969. This suggests that S3969 did not fully activate ENaC under our experimental conditions. A likely explanation for this finding is that the S3969 concentration used in the present study (10 μM) was not sufficient to achieve a maximal stimulation. Indeed, Lu et al. (36) reported a maximal stimulation of ENaC by S3969 at a threefold higher concentration (30 μM) (36) than that used in the present study. Importantly, βV348M-ENaC could also be stimulated by S3969. This demonstrates that the βV348M mutation has no impact on the stimulatory effect of S3969 on ENaC.

To further elucidate the molecular mechanism by which the βV348M mutation causes an increase in average channel P_o, we tested the functional effect of different amino acid substitutions at the βV348 residue on ENaC function. Interestingly, substitution of the βV348 residue by several amino acids resulted in ENaC stimulation. However, this effect could not be correlated to the size or charge of the amino acids. Therefore, we used computational channel modeling to analyze the putative microdomain around βV348. The results of this modeling suggest a qualitative correlation between the structural effect of the mutants and the observed effect on ΔI_{ami}. Mutants that destabilize the closed ENaC structure (V348 → G, K, M, L, W) generally result in increased ΔI_{ami}, whereas stabilizing mutants do not affect (V348E) or even reduce ΔI_{ami} (V348D). Therefore, it is tempting to speculate that mutants at position 348 that destabilize the closed ENaC conformation facilitate the closed to open transition, thereby increasing the open probability of the channel. This may also explain our experimental finding that the βV348M mutation reduced the number of channel transitions per second in single-channel recordings. A thorough structural interpretation of this effect, however, has to await the crystal structure of an open channel, which is currently not available.

Epithelia of conducting airways are covered by a mucus layer, which not only prevents desiccation but also scavenges inhaled particles. The mucus layer floats on a liquid or gel-like layer, the so-called periciliary layer (PCL), and is transported by cilia to the pharynx, where it is removed from the airways by coughing or swallowing, a process termed mucociliary clearance. Together, the mucus layer and the PCL are often referred to as the ASL layer (6). A well-defined microenvironment is essential for proper cilia function. In cultured human airway epithelial cells from healthy donors, the PCL was found to have the same height as that of outstretched cilia (~7 μm), whereas the height of the PCL was largely reduced (~3 μm) in cultured airway epithelial cells from patients with CF (38). Flattening of the PCL leads to steric hindrance of the cilia and thus impairs mucociliary clearance (32). Precise regulation of ASL volume is therefore an important prerequisite for proper lung defense. Interestingly, PCL height was similar in excised tracheal epithelia from newborn non-CF and $CFTR^{-/-}$ pigs, which had not yet developed airway inflammation (9). Thus it is still unclear whether flattening of the PCL in patients with CF occurs before the onset of inflammation or whether inflammation occurs first and affects transepithelial electrolyte transport, which then reduces PCL height. The gain-of-function effect of the βV348M mutation could favor disease in both situations. On the one hand, increased Na^+ absorption via overactive ENaC could flatten the PCL and thus reduce mucociliary clearance. On the other hand, the βV348M mutation could increase the vulnerability of airway epithelia to inflammatory processes by reducing the threshold for development of CF symptoms and thus influence the manifestation and intensity of the disease. In this context, it is of interest that the patient reported by Mutesa et al. (39) was compound heterozygous for the βV348M mutation and a F693L-CFTR mutation. The F693L-CFTR mutation was described as a polymorphism that, compared with wild-type CFTR, did not affect channel maturation in COS1 cells or chloride transport ability in oocytes (57). Therefore, it seems unlikely that the F693L-CFTR mutation alone is sufficient to cause the disease. However, in combination with the βV348M-ENaC gain-of-function mutation, it may contribute to the development and/or manifestation of CF disease.

In summary, we have shown that the βV348M mutation found in a patient with severe CF-like symptoms (39) stimulates ENaC activity by an increase in average channel P_o. The underlying mechanism for this increase is probably a destabilization of the closed channel state by the mutation. Our finding that the βV348M mutation has a gain-of-function effect may provide an explanation for the symptoms of the affected patient according to the pathophysiological concept that elevated Na^+ transport reduces mucociliary clearance in respiratory epithelia and favors CF-like pulmonary symptoms. However, additional factors may contribute to the patient's phenotype, and further studies are needed to elucidate the role of ENaC in the pathophysiology of CF.

ACKNOWLEDGMENTS

We acknowledge the expert technical assistance of Céline Grüninger, Sonja Mayer, Jessica Rinke, and Ralf Rinke. We thank Morag Mansley for proofreading the manuscript. Part of the study was published in abstract form (Soell et al. 2010, Acta Physiol 198, Suppl. 677: P-Tue-24).

GRANTS

This study was supported by the Johannes und Frieda Marohn-Stiftung at the Friedrich-Alexander-Universität Erlangen-Nürnberg.

DISCLOSURES

No conflicts of interest, financial or otherwise, are declared by the authors.

AUTHOR CONTRIBUTIONS

Author contributions: R.R. and C.K. conception and design of research; R.R., D.S., S.H., A.D., V.N., and B.K. performed experiments; R.R., D.S., A.D., V.N., and H.S. analyzed data; R.R., D.S., S.H., A.D., V.N., H.S., and C.K. interpreted results of experiments; R.R., D.S., A.D., V.N., and H.S. prepared figures; R.R. drafted manuscript; R.R., S.H., H.S., and C.K. edited and revised manuscript; R.R., D.S., S.H., A.D., V.N., B.K., H.S., and C.K. approved final version of manuscript.

REFERENCES

1. **Azad AK, Rauh R, Vermeulen F, Jaspers M, Korbmacher J, Boissier B, Bassinet L, Fichou Y, Georges MD, Stanke F, De Boeck K, Dupont L, Balascakova M, Hjelte L, Lebecque P, Radojkovic D, Castellani C, Schwartz M, Stuhrmann M, Schwarz M, Skalicka V, de Monestrol I, Girodon E, Ferec C, Claustres M, Tümmler B, Cassiman JJ, Korbmacher C, Cuppens H.** Mutations in the amiloride-sensitive epithelial sodium channel in patients with cystic fibrosis-like disease. *Hum Mutat* 30: 1093–1103, 2009.
2. **Boase NA, Rychkov GY, Townley SL, Dinudom A, Candi E, Voss AK, Tsoutsman T, Semsarian C, Melino G, Koentgen F, Cook DI, Kumar S.** Respiratory distress and perinatal lethality in Nedd4–2-deficient mice. *Nat Commun* 2: 287, 2011.
3. **Boucher RC.** Cystic fibrosis: a disease of vulnerability to airway surface dehydration. *Trends Mol Med* 13: 231–240, 2007.

4. **Bridges RJ, Newton BB, Pilewski JM, Devor DC, Poll CT, Hall RL.** Na^+ transport in normal and CF human bronchial epithelial cells is inhibited by BAY 39–9437. *Am J Physiol Lung Cell Mol Physiol* 281: L16–L23, 2001.
5. **Butterworth MB, Zhang L, Heidrich EM, Myerburg MM, Thibodeau PH.** Activation of the epithelial sodium channel (ENaC) by the alkaline protease from Pseudomonas aeruginosa. *J Biol Chem* 287: 32556–32565, 2012.
6. **Button B, Boucher RC.** Role of mechanical stress in regulating airway surface hydration and mucus clearance rates. *Respir Physiol Neurobiol* 163: 189–201, 2008.
7. **Caldwell RA, Boucher RC, Stutts MJ.** Neutrophil elastase activates near-silent epithelial Na^+ channels and increases airway epithelial Na^+ transport. *Am J Physiol Lung Cell Mol Physiol* 288: L813–L819, 2005.
8. **Caldwell RA, Boucher RC, Stutts MJ.** Serine protease activation of near-silent epithelial Na^+ channels. *Am J Physiol Cell Physiol* 286: C190–C194, 2004.
9. **Chen JH, Stoltz DA, Karp PH, Ernst SE, Pezzulo AA, Moninger TO, Rector MV, Reznikov LR, Launspach JL, Chaloner K, Zabner J, Welsh MJ.** Loss of anion transport without increased sodium absorption characterizes newborn porcine cystic fibrosis airway epithelia. *Cell* 143: 911–923, 2010.
10. **Chraibi A, Vallet V, Firsov D, Hess SK, Horisberger JD.** Protease modulation of the activity of the epithelial sodium channel expressed in Xenopus oocytes. *J Gen Physiol* 111: 127–138, 1998.
11. **Coote K, Atherton-Watson HC, Sugar R, Young A, MacKenzie-Beevor A, Gosling M, Bhalay G, Bloomfield G, Dunstan A, Bridges RJ, Sabater JR, Abraham WM, Tully D, Pacoma R, Schumacher A, Harris J, Danahay H.** Camostat attenuates airway epithelial sodium channel function in vivo through the inhibition of a channel-activating protease. *J Pharmacol Exp Ther* 329: 764–774, 2009.
12. **Davies J, Alton E, Griesenbach U.** Cystic fibrosis modifier genes. *J R Soc Med* 98, *Suppl* 45: 47–54, 2005.
13. **De Boeck K, Wilschanski M, Castellani C, Taylor C, Cuppens H, Dodge J, Sinaasappel M.** Cystic fibrosis: terminology and diagnostic algorithms. *Thorax* 61: 627–635, 2006.
14. **Diakov A, Bera K, Mokrushina M, Krueger B, Korbmacher C.** Cleavage in the γ-subunit of the epithelial sodium channel (ENaC) plays an important role in the proteolytic activation of near-silent channels. *J Physiol* 586: 4587–4608, 2008.
15. **Diakov A, Korbmacher C.** A novel pathway of epithelial sodium channel activation involves a serum- and glucocorticoid-inducible kinase consensus motif in the C terminus of the channel's α-subunit. *J Biol Chem* 279: 38134–38142, 2004.
16. **Donaldson SH, Boucher RC.** Sodium channels and cystic fibrosis. *Chest* 132: 1631–1636, 2007.
17. **Donaldson SH, Hirsh A, Li DC, Holloway G, Chao J, Boucher RC, Gabriel SE.** Regulation of the epithelial sodium channel by serine proteases in human airways. *J Biol Chem* 277: 8338–8345, 2002.
18. **Eaton DC, Helms MN, Koval M, Bao HF, Jain L.** The contribution of epithelial sodium channels to alveolar function in health and disease. *Annu Rev Physiol* 71: 403–423, 2009.
19. **Garty H, Palmer LG.** Epithelial sodium channels: function, structure, and regulation. *Physiol Rev* 77: 359–396, 1997.
20. **Gentzsch M, Dang H, Dang Y, Garcia-Caballero A, Suchindran H, Boucher RC, Stutts MJ.** The cystic fibrosis transmembrane conductance regulator impedes proteolytic stimulation of the epithelial Na^+ channel. *J Biol Chem* 285: 32227–32232, 2010.
21. **Haerteis S, Krappitz M, Diakov A, Krappitz A, Rauh R, Korbmacher C.** Plasmin and chymotrypsin have distinct preferences for channel activating cleavage sites in the γ subunit of the human epithelial sodium channel. *J Gen Physiol* 140: 375–389, 2012.
22. **Haerteis S, Krueger B, Korbmacher C, Rauh R.** The δ-subunit of the epithelial sodium channel (ENaC) enhances channel activity and alters proteolytic ENaC activation. *J Biol Chem* 284: 29024–29040, 2009.
23. **Harris M, Firsov D, Vuagniaux G, Stutts MJ, Rossier BC.** A novel neutrophil elastase inhibitor prevents elastase activation and surface cleavage of the epithelial sodium channel expressed in Xenopus laevis oocytes. *J Biol Chem* 282: 58–64, 2007.
24. **Huber R, Krueger B, Diakov A, Korbmacher J, Haerteis S, Einsiedel J, Gmeiner P, Azad AK, Cuppens H, Cassiman JJ, Korbmacher C, Rauh R.** Functional characterization of a partial loss-of-function mutation of the epithelial sodium channel (ENaC) associated with atypical cystic fibrosis. *Cell Physiol Biochem* 25: 145–158, 2010.
25. **Itani OA, Chen JH, Karp PH, Ernst S, Keshavjee S, Parekh K, Klesney-Tait J, Zabner J, Welsh MJ.** Human cystic fibrosis airway epithelia have reduced Cl^- conductance but not increased Na^+ conductance. *Proc Natl Acad Sci USA* 108: 10260–10265, 2011.
26. **Jasti J, Furukawa H, Gonzales EB, Gouaux E.** Structure of acid-sensing ion channel 1 at 1.9 Å resolution and low pH. *Nature* 449: 316–323, 2007.
27. **Kellenberger S, Gautschi I, Rossier BC, Schild L.** Mutations causing Liddle syndrome reduce sodium-dependent downregulation of the epithelial sodium channel in the Xenopus oocyte expression system. *J Clin Invest* 101: 2741–2750, 1998.
28. **Kellenberger S, Gautschi I, Schild L.** An external site controls closing of the epithelial Na^+ channel ENaC. *J Physiol* 543: 413–424, 2002.
29. **Kellenberger S, Schild L.** Epithelial sodium channel/degenerin family of ion channels: a variety of functions for a shared structure. *Physiol Rev* 82: 735–767, 2002.
30. **Kimura T, Kawabe H, Jiang C, Zhang W, Xiang YY, Lu C, Salter MW, Brose N, Lu WY, Rotin D.** Deletion of the ubiquitin ligase Nedd4L in lung epithelia causes cystic fibrosis-like disease. *Proc Natl Acad Sci USA* 108: 3216–3221, 2011.
31. **Kleyman TR, Carattino MD, Hughey RP.** ENaC at the cutting edge: regulation of epithelial sodium channels by proteases. *J Biol Chem* 284: 20447–20451, 2009.
32. **Knowles MR, Boucher RC.** Mucus clearance as a primary innate defense mechanism for mammalian airways. *J Clin Invest* 109: 571–577, 2002.
33. **Korbmacher C, Volk T, Segal AS, Boulpaep EL, Frömter E.** A calcium-activated and nucleotide-sensitive nonselective cation channel in M-1 mouse cortical collecting duct cells. *J Membr Biol* 146: 29–45, 1995.
34. **Krueger B, Haerteis S, Yang L, Hartner A, Rauh R, Korbmacher C, Diakov A.** Cholesterol depletion of the plasma membrane prevents activation of the epithelial sodium channel (ENaC) by SGK1. *Cell Physiol Biochem* 24: 605–618, 2009.
35. **Lazrak A, Jurkuvenaite A, Chen L, Keeling KM, Collawn JF, Bedwell DM, Matalon S.** Enhancement of alveolar epithelial sodium channel activity with decreased cystic fibrosis transmembrane conductance regulator expression in mouse lung. *Am J Physiol Lung Cell Mol Physiol* 301: L557–L567, 2011.
36. **Lu M, Echeverri F, Kalabat D, Laita B, Dahan DS, Smith RD, Xu H, Staszewski L, Yamamoto J, Ling J, Hwang N, Kimmich R, Li P, Patron E, Keung W, Patron A, Moyer BD.** Small molecule activator of the human epithelial sodium channel. *J Biol Chem* 283: 11981–11994, 2008.
37. **Mall M, Grubb BR, Harkema JR, O'Neal WK, Boucher RC.** Increased airway epithelial Na^+ absorption produces cystic fibrosis-like lung disease in mice. *Nat Med* 10: 487–493, 2004.
38. **Matsui H, Grubb BR, Tarran R, Randell SH, Gatzy JT, Davis CW, Boucher RC.** Evidence for periciliary liquid layer depletion, not abnormal ion composition, in the pathogenesis of cystic fibrosis airways disease. *Cell* 95: 1005–1015, 1998.
39. **Mutesa L, Azad AK, Verhaeghe C, Segers K, Vanbellinghen JF, Ngendahayo L, Rusingiza EK, Mutwa PR, Rulisa S, Koulischer L, Cassiman JJ, Cuppens H, Bours V.** Genetic analysis of Rwandan patients with cystic fibrosis-like symptoms: identification of novel cystic fibrosis transmembrane conductance regulator and epithelial sodium channel gene variants. *Chest* 135: 1233–1242, 2009.
40. **Myerburg MM, Butterworth MB, McKenna EE, Peters KW, Frizzell RA, Kleyman TR, Pilewski JM.** Airway surface liquid volume regulates ENaC by altering the serine protease-protease inhibitor balance: A mechanism for sodium hyperabsorption in cystic fibrosis. *J Biol Chem* 281: 27942–27949, 2006.
41. **Nesterov V, Dahlmann A, Bertog M, Korbmacher C.** Trypsin can activate the epithelial sodium channel (ENaC) in microdissected mouse distal nephron. *Am J Physiol Renal Physiol* 295: F1052–F1062, 2008.
42. **Nesterov V, Dahlmann A, Krueger B, Bertog M, Loffing J, Korbmacher C.** Aldosterone dependent and independent regulation of the epithelial sodium channel (ENaC) in mouse distal nephron. *Am J Physiol Renal Physiol*. In press.
43. **Planes C, Leyvraz C, Uchida T, Angelova MA, Vuagniaux G, Hummler E, Matthay M, Clerici C, Rossier B.** In vitro and in vivo regulation of transepithelial lung alveolar sodium transport by serine proteases. *Am J Physiol Lung Cell Mol Physiol* 288: L1099–L1109, 2005.
44. **Rauh R, Diakov A, Tzschoppe A, Korbmacher J, Azad AK, Cuppens H, Cassiman JJ, Dotsch J, Sticht H, Korbmacher C.** A mutation of the epithelial sodium channel associated with atypical cystic fibrosis increases

channel open probability and reduces Na^+ self inhibition. *J Physiol* 588: 1211–1225, 2010.
45. **Rauh R, Dinudom A, Fotia AB, Paulides M, Kumar S, Korbmacher C, Cook DI.** Stimulation of the epithelial sodium channel (ENaC) by the serum- and glucocorticoid-inducible kinase (Sgk) involves the PY motifs of the channel but is independent of sodium feedback inhibition. *Pflügers Arch* 452: 290–299, 2006.
46. **Riordan JR, Rommens JM, Kerem B, Alon N, Rozmahel R, Grzelczak Z, Zielenski J, Lok S, Plavsic N, Chou JL, Drumm ML, Ianuzzi C, Collins FS, Tsui LC.** Identification of the cystic fibrosis gene: cloning and characterization of complementary DNA. *Science* 245: 1066–1073, 1989.
47. **Rossier BC, Stutts MJ.** Activation of the epithelial sodium channel (ENaC) by serine proteases. *Annu Rev Physiol* 71: 361–379, 2009.
48. **Sayle RA, Milner-White EJ.** RASMOL: biomolecular graphics for all. *Trends Biochem Sci* 20: 374, 1995.
49. **Schwede T, Kopp J, Guex N, Peitsch MC.** SWISS-MODEL: An automated protein homology-modeling server. *Nucleic Acids Res* 31: 3381–3385, 2003.
50. **Sheppard DN, Welsh MJ.** Structure and function of the CFTR chloride channel. *Physiol Rev* 79: S23–S45, 1999.
51. **Sheridan MB, Fong P, Groman JD, Conrad C, Flume P, Diaz R, Harris C, Knowles M, Cutting GR.** Mutations in the beta-subunit of the epithelial Na^+ channel in patients with a cystic fibrosis-like syndrome. *Hum Mol Genet* 14: 3493–3498, 2005.
52. **Snyder PM, Bucher DB, Olson DR.** Gating induces a conformational change in the outer vestibule of ENaC. *J Gen Physiol* 116: 781–790, 2000.
53. **Stanke F, Becker T, Cuppens H, Kumar V, Cassiman JJ, Jansen S, Radojkovic D, Siebert B, Yarden J, Ussery DW, Wienker TF, Tümmler B.** The TNFα receptor TNFRSF1A and genes encoding the amiloride-sensitive sodium channel ENaC as modulators in cystic fibrosis. *Hum Genet* 119: 331–343, 2006.
54. **Stewart AP, Haerteis S, Diakov A, Korbmacher C, Edwardson JM.** Atomic force microscopy reveals the architecture of the epithelial sodium channel (ENaC). *J Biol Chem* 286: 31944–31952, 2011.
55. **Stockand JD, Staruschenko A, Pochynyuk O, Booth RE, Silverthorn DU.** Insight toward epithelial Na^+ channel mechanism revealed by the acid-sensing ion channel 1 structure. *IUBMB Life* 60: 620–628, 2008.
56. **Tarran R, Trout L, Donaldson SH, Boucher RC.** Soluble mediators, not cilia, determine airway surface liquid volume in normal and cystic fibrosis superficial airway epithelia. *J Gen Physiol* 127: 591–604, 2006.
57. **Vankeerberghen A, Wei L, Jaspers M, Cassiman JJ, Nilius B, Cuppens H.** Characterization of 19 disease-associated missense mutations in the regulatory domain of the cystic fibrosis transmembrane conductance regulator. *Hum Mol Genet* 7: 1761–1769, 1998.
58. **Wielpütz MO, Lee IH, Dinudom A, Boulkroun S, Farman N, Cook DI, Korbmacher C, Rauh R.** NDRG2 stimulates amiloride-sensitive Na^+ currents in Xenopus laevis oocytes and Fisher rat thyroid cells. *J Biol Chem* 282: 28264–28273, 2007.
59. **Zhou Z, Treis D, Schubert SC, Harm M, Schatterny J, Hirtz S, Duerr J, Boucher RC, Mall MA.** Preventive but not late amiloride therapy reduces morbidity and mortality of lung disease in βENaC-overexpressing mice. *Am J Respir Crit Care Med* 178: 1245–1256, 2008.